






Article

Novel Fuzzy-Based Optimization Approaches for the Prediction of Ultimate Axial Load of Circular Concrete-Filled Steel Tubes

Jinsong Liao ^{1,*}, Panagiotis G. Asteris ^{2,*} , Liborio Cavaleri ³, Ahmed Salih Mohammed ⁴ , Minas E. Lemonis ² , Markos Z. Tsoukalas ², Athanasia D. Skentou ², Chrysanthos Maraveas ⁵ , Mohammadreza Koopialipoor ⁶ and Danial Jahed Armaghani ⁷ 

¹ School of Construction Management, Chongqing Jianzhu College, Chongqing 400072, China

² Computational Mechanics Laboratory, School of Pedagogical and Technological Education, 14121 Athens, Greece; mlemonis@hotmail.com (M.E.L.); tsoukalas6967@gmail.com (M.Z.T.); athanasiaskentou@hotmail.gr (A.D.S.)

³ Department of Engineering, University of Palermo, 90133 Palermo, Italy; liborio.cavaleri@unipa.it

⁴ Civil Engineering Department, College of Engineering, University of Sulaimani, Sulaymaniyah 46001, Iraq; ahmed.mohammed@univsul.edu.iq

⁵ Farm Structures Laboratory, Department of Natural Resources and Agricultural Engineering, Agricultural University of Athens, 11855 Athens, Greece; c.maraveas@maraveas.gr

⁶ Faculty of Civil and Environmental Engineering, Amirkabir University of Technology, Tehran 15914, Iran; mr.koopialipoor@aut.ac.ir

⁷ Department of Urban Planning, Engineering Networks and Systems, Institute of Architecture and Construction, South Ural State University, 76, Lenin Prospect, 454080 Chelyabinsk, Russia; danialarmaghani@susu.ru

* Correspondence: liaojinsong1022@163.com (J.L.); asteris@aspete.gr (P.G.A.)



Citation: Liao, J.; Asteris, P.G.; Cavaleri, L.; Mohammed, A.S.; Lemonis, M.E.; Tsoukalas, M.Z.; Skentou, A.D.; Maraveas, C.; Koopialipoor, M.; Armaghani, D.J. Novel Fuzzy-Based Optimization Approaches for the Prediction of Ultimate Axial Load of Circular Concrete-Filled Steel Tubes. *Buildings* **2021**, *11*, 629. <https://doi.org/10.3390/buildings11120629>

Academic Editor: David Arditi

Received: 6 November 2021

Accepted: 7 December 2021

Published: 9 December 2021

Publisher's Note: MDPI stays neutral with regard to jurisdictional claims in published maps and institutional affiliations.



Copyright: © 2021 by the authors. Licensee MDPI, Basel, Switzerland. This article is an open access article distributed under the terms and conditions of the Creative Commons Attribution (CC BY) license (<https://creativecommons.org/licenses/by/4.0/>).

Abstract: An accurate estimation of the axial compression capacity of the concrete-filled steel tubular (CFST) column is crucial for ensuring the safety of structures containing them and preventing related failures. In this article, two novel hybrid fuzzy systems (FS) were used to create a new framework for estimating the axial compression capacity of circular CCFST columns. In the hybrid models, differential evolution (DE) and firefly algorithm (FFA) techniques are employed in order to obtain the optimal membership functions of the base FS model. To train the models with the new hybrid techniques, i.e., FS-DE and FS-FFA, a substantial library of 410 experimental tests was compiled from openly available literature sources. The new model's robustness and accuracy was assessed using a variety of statistical criteria both for model development and for model validation. The novel FS-FFA and FS-DE models were able to improve the prediction capacity of the base model by 9.68% and 6.58%, respectively. Furthermore, the proposed models exhibited considerably improved performance compared to existing design code methodologies. These models can be utilized for solving similar problems in structural engineering and concrete technology with an enhanced level of accuracy.

Keywords: CCFST; hybrid; prediction; FFA; DE; FS

1. Introduction

Concrete-filled steel tube (CFST) members make better utilization of steel and concrete than traditional bare steel or reinforced concrete structures. The steel tube gives confinement to the concrete infill, while the concrete infill prevents the inward buckling of the steel tube. CFST members have a long history of being used in a broad range of construction projects due to their efficiency as structural components. As an example, CFSTs have been utilized as (1) mega columns in super high-rise buildings, (2) chord members in long-span arch bridges, (3) bridge piers, (4) floodwall piling, and (5) underwater pipeline structures, as described by researchers like Wang et al. [1]. For the most part, the CFST components in these situations are utilized to support compressive forces.

When it comes to improving the compressive strength of CFST components, there are primarily two approaches that are used. Using bigger cross sections is one approach. However, it may increase structural weight (and as a result the seismic impact) and decrease useable space, making it a less feasible or cost-effective solution. Alternatively, high strength steel (i.e., with a yield stress higher than 525 MPa) and high strength concrete (i.e., with a compressive strength greater than 70 MPa) are two additional viable methods [AISC 360 [2]].

According to experts like Nishiyama et al. [3], Kim [4] and Han [5] and others, many studies have been carried out to examine the behavior of conventional-strength members of the CFST. Several researchers have experimented with the behavior of high-strength CFST columns facilitating their adoption in practice. For example, Cederwall et al. [6], Varma [7], Uy [8], Liu et al. [9], Mursi and Uy [10], Sakino et al. [11], Lue et al. [12], Aslani et al. [13], and Xiong et al. [14] have performed experimental testing on high-strength rectangular CFST short columns. Lai and Varma [15] reviewed these experiments and provided design equations for calculating the cross-sectional strength of high-strength rectangular CFST columns and also effective stress-strain relationships for the steel tube and concrete infill of such high-strength components.

Additional experimental tests on CFST columns were conducted by Gardner and Jacobson [16], Bergmann [17], O’Shea and Bridge [18], Schneider [19], O’Shea and Bridge [20], Giakoumelis and Lam [21], Sakino et al. [11], Zeghiche and Chaoui [22], Yu et al. [23], de Oliveira et al. [24], Liew and Xiong [25], Chen et al. [26]. The experimental results from previous studies have been employed in this study in order to build an experimental database. It is noted, however, that experiments featuring columns with fibers in the concrete, stainless or aluminum steel tubing, grease on the inner surface of the tubing, or concrete infill alone were excluded from this database.

Machine learning (ML) methods have been widely used in many civil engineering applications [27–55], particularly in compressive structures [56–59]. ML uses databases to develop models that can solve various linear and nonlinear problems with varying degrees of complexity. These methods, using computer processing, help considerably in solving problems more efficiently and quickly, and is introduced as a powerful alternative method for older, experimental and statistical models. An optimization and tree-based approach has been developed by Sarir et al. [60] to find out the maximum capacity of circular CFST members. Short CFST members’ load-bearing capacity was predicted by Ahmadi et al. using an artificial neural network [61,62]. A gene expression model for predicting circular CFST capability was established by Güneyisi et al. [63] and Ipek and Güneyisi [64]. In the study of Moon et al. [65], the load-bearing behavior of circular CFST was also examined using a fuzzy logic model. According to Al-Khaleefi et al. [66], the fire resistance of CFST columns has also been studied using a machine learning method that considers material characteristics and loading circumstances. For sections other than circular, Ren et al. [67] recently published a study on the prediction of square CFST members, using support vector machines and particle optimization methods. While for the same section Tran et al. [68] used a neural network model to predict the ultimate load. Also, Lee et al. [69] used a categorical gradient boosting algorithm to predict the strength of both circular and rectangular CFSTs under concentric or eccentric loading. Zarringol et al. [70] used ANN for the same problem. It can be concluded from these studies that ML methods prove quite promising in investigating the mechanical behavior of structures made up of CFST members.

In this research, the major goal is to develop a regression machine learning model for compressive circular CFST, particularly in contemporary buildings. This was achieved using a hybridizing fuzzy system (FS) with two optimization algorithms known as the firefly algorithm (FFA) and differential evolution (DE). The input data consist of column length, cross-section diameter and steel tube thickness in addition to concrete compressive and steel yield stress. Precise quality metrics such as root mean-squared-error (RMSE), and coefficient of determination (R^2) were utilized throughout the model’s testing/validation

phase. The FS-FFA and FS-DE models were evaluated and compared with existing design code methodologies to highlight the best predictive model for the examined problem.

2. Research Significance

CFST design can be done using different methods and codes around the world. Accurate, faster, and less costly design is one of the priorities of any structural project. Due to the fact that an accurate CFST design has important effects on the stability of structures, examining different techniques could give a better understanding of their effects and behaviour. Therefore, this research, using a new generation of computational methods developed by learning machines, is aimed at coming up with a practical solution to the aforementioned problem. Using a combination of FS and optimization algorithms (i.e., FFA and DE), new predictive models can be developed to more accurately and quickly evaluate CFST design. Optimal solutions of hybrid models consisting of these conditions can be used for new conditions and provide acceptable results considering practical applications in industrial fields.

3. Short Literature Review on Design Codes

The design of circular CFST columns is already supported by several steel and composite codes, available worldwide. Such codes include EN1994 [71] in Europe, AISC 360 [72] in the USA, AIJ [73] in Japan. Besides providing the squash load that is relevant for short columns, design codes also provide methodologies to predict the resistance against flexural buckling, which becomes the critical failure mode for long, slender columns. Local buckling of the steel tube is also a failure mode relevant for thin-walled steel sections. It is typically covered by placing section slenderness limits and depending on them, either accounting for a reduced effective steel sectional area (i.e., EN1994 [71]), or limiting the ultimate stress the composite section may reach (i.e., AISC 360 [72]). Regarding squash load, which involves the plastic strength of the steel and concrete parts of the CFST section, the influence of the increased concrete confinement provided by the circular tube is typically expressed through an increase of the concrete strength contribution. The following formulas describe the squash loads, for the EN1994 [71], AISC 360 [72], AIJ [73] design codes (ignoring any safety factors):

$$N_p^{EN1994} = \begin{cases} \eta_a f_y A_s + \left(1 + \eta_c \frac{t f_y}{d f'_c}\right) f'_c A_c & , \bar{\lambda} < 0.5 \\ f_y A_s + f'_c A_c & , \bar{\lambda} \geq 0.5 \end{cases} \quad (1)$$

$$N_p^{AISC360} = f_y A_s + 0.95 f'_c A_c \quad (2)$$

$$N_p^{AIJ} = 1.27 f_y A_s + 0.85 f'_c A_c \quad (3)$$

Factors η_a and η_c account for the member slenderness $\bar{\lambda}$. For slender columns, the squash loads given above fail to represent the ultimate compressive load. In such cases, buckling phenomena emerge that cause an earlier failure, depending on the global column slenderness. The methodologies provided by the aforementioned design codes are differentiated in this context. Due to space limitations the relevant expressions are not reproduced herein however.

All design codes place specific limits on their field of application. These are related to material strength limits, steel tube slenderness, global slenderness or steel to concrete ratio. Table 1 presents the relevant application limits for the codes examined.

Table 1. Design codes application limits, related to circular CFSTs.

Code	f_y (MPa)	f'_c (MPa)	Section Slenderness	Other
EN1994 [71]	$235 \leq f_y \leq 460$	$25 \leq f'_c \leq 50$	$\frac{d}{t} \leq 90 \frac{235 \text{ MPa}}{f_y}$	$0.2 \leq \frac{A_s f_y}{N_p} \leq 0.9$
AISC 360 [72]	$f_y \leq 525$	$21 \leq f'_c \leq 69$	$\frac{d}{t} \leq \frac{0.31 E_s}{f_y}$	$A_s \geq 0.01 A_{sc}$
AIJ [73]	$235 \leq f_y \leq 355$	$18 \leq f'_c \leq 60$	$\frac{d}{t} \leq 1.5 \frac{23500 \text{ MPa}}{\sqrt{\min\{f_y, 0.7 f_u\}}}$	$\frac{L_e}{B} \leq 50$

A_{sc} , A_s , and A_c are the areas of the total cross section, the steel tube and the concrete core, respectively L_e is the column effective length.

4. Modeling Approaches

4.1. Fuzzy System (FS)

A chapter titled “fuzzy sets” by Professor Lotfizadeh in 1965 presented the fuzzy theory [74]. Initially, his primary objective was to create a more accurate model of how natural language processing works. Fuzzy sets, fuzzy events, fuzzy numbers, and phases are only a few of the innovations he made to mathematics and engineering thanks to these ideas. A rule base, which includes If–Then rules created by application specialists, constitutes FS’s core component [75]. Membership functions are used to deploy the fuzzy sets. For the FS process, the most popular fuzzifiers are Gaussian, Singleton, and Triangular. In addition, the most often used defuzzifiers in the literature are center of gravity, center average, and maximum. Fuzzy logic principles govern the firing of If–Then rules while the inference engine is operating. A fuzzy rule has the following syntax [76]:

$$\text{If } x_1 \text{ is } A_1 \text{ and } \dots x_n \text{ is } A_n \text{ then } Y \text{ is } B \quad (4)$$

Fuzzy sets in U R (U is the input space) are A_i and V R (V is the output space) are B , and X is equal to the product of the variables in the input space and the variables in the output space, respectively. There are two types of FS controller: closed-loop and open-loop. The product inference engine and Gaussian fuzzifier were used in the following ways:

$$f_{1(x)} = \begin{cases} \exp\left[-\frac{1}{2}\left(\frac{x-m_1}{\sigma}\right)^2\right] & x \leq m_1 \\ 1 & \text{otherwise} \end{cases} \quad (5)$$

$$f_{2(x)} = \begin{cases} 1 & x \leq m_2 \\ \exp\left[-\frac{1}{2}\left(\frac{x-m_1}{\sigma}\right)^2\right] & \text{otherwise} \end{cases} \quad (6)$$

4.2. Firefly Algorithm (FFA)

Yang was the first to propose FFA as a nature-inspired, meta-heuristic algorithm [77]. Engineers have used this method to address a variety of issues. The most critical aspects of the FFA process are the formulation of attraction and the change in light intensity. Fireflies will operate virtually independently in FFA modelling, which is advantageous for parallel implementation in particular. Fireflies in this algorithm tend to congregate closer to the optimum, making it superior to the particle swarm optimization (PSO) and the genetic algorithm (GA) [76,78]. Figure 1 depicts FFA’s foundation for a better understanding. Several studies, including Yang [77], Zhang and Wu [79], and Apostolopoulos and Vlachos [80], go into great depth regarding FFA. Reviewing past research shows that the FFA may be utilized as a powerful tool for engineering optimization in almost all fields [81,82]. Gholizadeh and Barati [83], for example, used the PSO, FFA, and harmony search (HS) to explore the size and form optimization of truss systems. In terms of optimizing the size and geometry of truss structures, FFA outperformed PSO and HS.

```

START
Generate Initial population of fireflies  $\mathbf{x}=(x_1, \dots, x_n)$ 
Determine Intensity ( $I$ ) at objective function  $f(x_i)$ 
While  $t < \text{MaxIter}$ 
  For  $i=1:n$ 
    For  $j=1:n$ 
      If  $I_j > I_i$ 
        Move fireflies  $i$  and  $j$  in  $d$ -dimension
      End if
      Attractiveness varies with distance  $r$  via  $\exp[-\gamma r]$ 
      Evaluate new solution and update light intensity
    End
  End
  Rank the fireflies and find the current best
End
END

```

Figure 1. Base of firefly algorithm (FFA).

4.3. Differential Evolution (DE)

Storn and Price (1997) first proposed the concept of differential evolution (DE) as a stochastic population-based search technique [84]. NP members are randomly selected from the original population (parents) before the search may begin. Using crossover, mutation, and selection operators, the DE technique then produces a new population (i.e., offspring). This iteration's members are chosen by comparing how similar they are to the previous iteration's members. This cycle is repeated until the desired outcome is achieved. The following sections describe the major stages of this algorithm [84].

4.3.1. Generating the Initial Population

If the problem's decision variables are indicated by D , the initial population vector is produced with a random size $N \times D$ inside the decision variables allowed range, according to the following equation:

$$x_{i0} = x_{imin} + \text{round}(\varphi_i \times x_{imax} - x_{imin}), \quad i = 1, \dots, NP \quad (7)$$

There are lower and higher limits on the choice variables x_{imin} and x_{imax} , respectively, while index i is a random number between 0 and 1.

4.3.2. Mutation

To carry out the mutation procedure, the following equation is used:

$$v_{i,G+1} = x_{r1,G} + F \times (x_{r2,G} - x_{r3,G}) \quad (8)$$

There are three randomly selected members of the population in this case, and the scaling factor F ranges from zero to two, giving us a mutant vector $v_{i,G+1}$ and three randomly picked members of the population.

4.3.3. Crossover

This operator combines the modified particles with the members of the target group that were chosen in the first stage as follows:

$$u_{ij,G+1} = \begin{cases} v_{ji,G+1} & r < Cr \text{ or } j = rn_i \\ x_{ji,G} & \text{otherwise} \end{cases} \quad (9)$$

where $j = 1, 2, \dots, D$; $r_j \in [0, 1]$ is the random number; C_r stands for the crossover constant $\in [0, 1]$; and $\in rn_i (1, 2, \dots, D)$ is the randomly chosen index.

4.3.4. Selection

Once all operators have been initialised to their respective goal functions, a new measurement vector and target member are created. If the measurement vector's value exceeds the target member's, the member is promoted to the next generation. If this does not happen, the target member will be added to the population of the following generation. Figure 2 depicts the DE's pseudo-code.

```

START
Initialize the random population  $X_i, G i=1, \dots, NP$ 
Evaluate  $f(X_i, G) i=1, \dots, NP$ 
For  $G=1:MaxIter$ 
  For  $i=1:NP$ 
    Select randomly  $x_{r1,G}, x_{r2,G}, x_{r3,G}$ 
    For  $j=1:D$ 
      If  $rand_j (0,1) < CR$ 
         $v_{ji,G+1} = x_{r1,G} + F \times (x_{r2,G} - x_{r3,G})$ 
      Else
         $v_{ji,G+1} = x_{ji,G}$ 
      End if
    End For
    If  $f(v_{ji,G+1}) \leq f(X_i, G)$ 
       $x_{i,G+1} = v_{i,G+1}$ 
    Else
       $x_{i,G+1} = x_{i,G}$ 
    End if
  End for
End For
END

```

Figure 2. Pseudo-code of the differential evolution (DE).

4.4. Hybridization of FS

The CCFST is predicted using two hybrid FS-FFA and FS-DE in this research. Five characteristics were utilized as inputs in the hybrid FS modelling procedure, with CCFST ultimate load being the output. The proposed FS-FFA and FS-DE models were trained and tested using 328 datasets of data in the training phase and 82 datasets of data in the testing phase. Fuzzy-based modifications to FFA and DE are suggested in this research to remove or minimize model drawbacks. In this structure, the member (population) of optimization algorithms in each step may affect each other's movements. For determining progress in the program, we used two metrics to indicate how close the algorithms are getting to the ideal answer. We call this loop counter (iteration) Count and its value is decided by

expertise or via trial and error [85]. The fuzzy controller will have to deal with this last problem. The following is an introduction to the delta parameter:

$$\Delta^i = F(\text{Best}^i) - F(\text{TBest}^{i-1}) \quad (10)$$

Iteration i yields Best^i , which is the best solution, whereas iteration $i-1$ yields TBest^{i-1} , which is the best solution. One of the benefits of the hybrid FS is that it regulates the fundamental database, i.e., physics of the examined problem. As a result, convergence speed may be improved by making the appropriate initial adjustments. A MATLAB programme was used to implement the hybrid FS model's code. The following equation is used to standardize datasets before beginning hybrid FS modelling:

$$X_{\text{norm}} = \frac{X - X_{\text{min}}}{X_{\text{max}} - X_{\text{min}}} \quad (11)$$

where X , X_{min} , and X_{max} represent the parameters' real values, minimum and maximum values, respectively, while X_{norm} represents the parameter's normalized value. FS-FFA modeling's most critical parameters are Npop (swarm size), Alpha (mutation coefficient), Gamma (light absorption coefficient), Beta (attraction coefficient base value) and Maxiter (maximum number of iterations), according to prior research [81,82,85]. Parameters' number of iteration, crossover constant and population (Npop) are also effective for the DE algorithm [84,86]. Following the trial and error technique, Npop of FFA was set to 50, Npop of DE was set to 80, Alpha was set to 0.25, Gamma was set to 1, crossover constant was set to 0.8, Beta was set to 2, and the number of iterations for both algorithms was set to 500. Figure 3 depicts the steps involved in putting hybrid FS into practice.

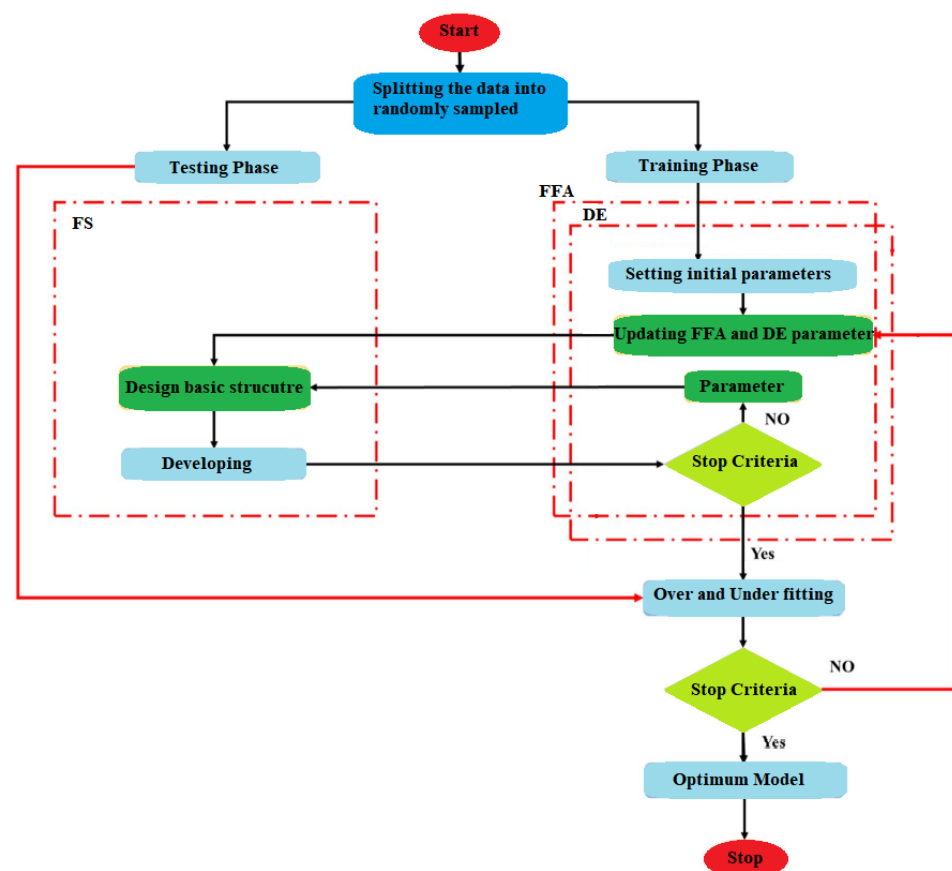


Figure 3. The general flowchart developed in this research.

5. Data Setup

A variety of sources were used to compile the database for this study such as Wang et al. [87], Geng [88], Dong et al. [89], Wang et al. [90], Chen et al. [91], Yang et al. [92], Wang et al. [93], Wei et al. [94] Hoang and Fehling [95], He et al. [96]. These sources include axial compression tests on circular CFST columns that make up 410 samples in total (whole used datasets for modeling are presented in Appendix A). Several geometrical factors and mechanical characteristics were utilized in these tests to investigate the failure of CFST columns under axial stress. These are column length (L), diameter (D), and thickness (t) as geometrical input variables. Additionally, the steel tube yield stress (f_y) and the compressive strength (f_c) of the filling concrete are the material specific variables representing their mechanical properties. The only output of the problem is the CFST column ultimate experimental axial compressive load (Pexp). Table 2 shows a statistical examination of the dataset.

Table 2. General information of dataset.

Parameter	Unit	Min	Average	Max	SDT
L	mm	180	720.73	4000	594.56
D	mm	60	169.41	550	74.04
t	mm	0.86	4.47	16.72	2.59
f_y	MPa	184.8	388.38	1153	170.29
f_c	MPa	23.2	74.98	188.1	44.01
Pexp	KN	215	2992.71	29590	3213.2

6. Development of the Hybrid Models

The performance of FS-FFA and FS-DE models is discussed in this part, presenting how well it can predict the circular CFST ultimate compressive load. In order to do this, three quantitative standard statistical performance measures, namely R^2 , the a20-index, and RMSE, have been used, as described by Equations (12)–(14) [52,58,97–102]:

$$RMSE = \sqrt{\frac{1}{n} \sum_{i=1}^n (y_{fr,i} - \hat{y}_{fr,i})^2} \quad (12)$$

$$R^2 = 1 - \frac{\sum_{i=1}^n (y_{fr,i} - \hat{y}_{fr,i})^2}{\sum_{i=1}^n (y_{fr,i} - \bar{y}_{fr,i})^2} \quad (13)$$

$$a20 - index = \frac{m20}{n} \quad (14)$$

where, the predicted and measured values for n data are indicated by $\hat{y}_{fr,i}$ and $y_{fr,i}$, respectively, and m20 is the number of samples with a value of (experimental value)/(predicted value) ratio, between 0.80 and 1.20. The best performance of the models is achieved when the errors (RMSE) are zero and the R^2 is close to one. The performance of the developed FS-FFA and FS-DE is presented in Table 3 in terms of R^2 , RMSE, and a20-index. The optimal model values have been optimally picked having as objective to achieve the best possible performance metrics.

Table 3. The final result of hybrid fuzzy system (FS) models.

Model	Training			Testing		
	a20-Index	R^2	RMSE	a20-Index	R^2	RMSE
FS-FFA	0.9604	0.9854	482.0362	0.8659	0.9880	415.4471
FS-DE	0.9634	0.9571	655.4708	0.8659	0.9876	419.4502

In Table 3, it can be shown that the proposed FS-FFA and FS-DE have a good performance for predicting CFST values. In the training section, the performance of the FS-FFA model seems better in terms of RMSE and a20-index, compared to the FS-DE model whereas the latter scores a higher R^2 value. However, in the test section, the performance of the two models proves more closely matched, with the FS-FFA achieving slightly better metrics. Given that the FS-FFA model has been able to provide better predictions in both sections, it becomes the preferred one for the estimation of circular CFST ultimate compressive load. Figures 4 and 5 show separately for the training and the testing datasets graphs of predicted vs. experimental loads for both hybrid models. It can be seen that both models exhibit a consistent performance throughout the range of available compressive loads.

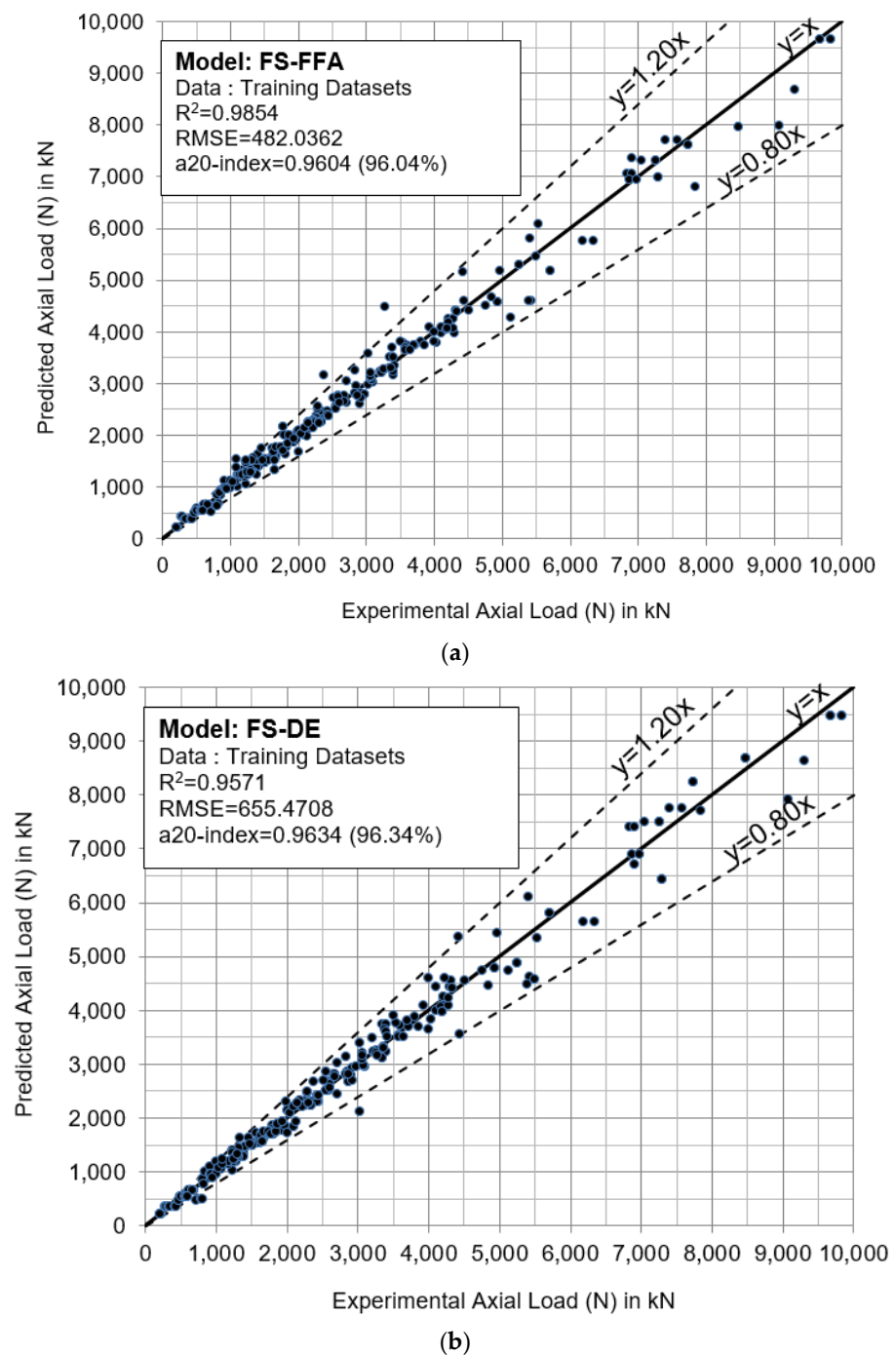
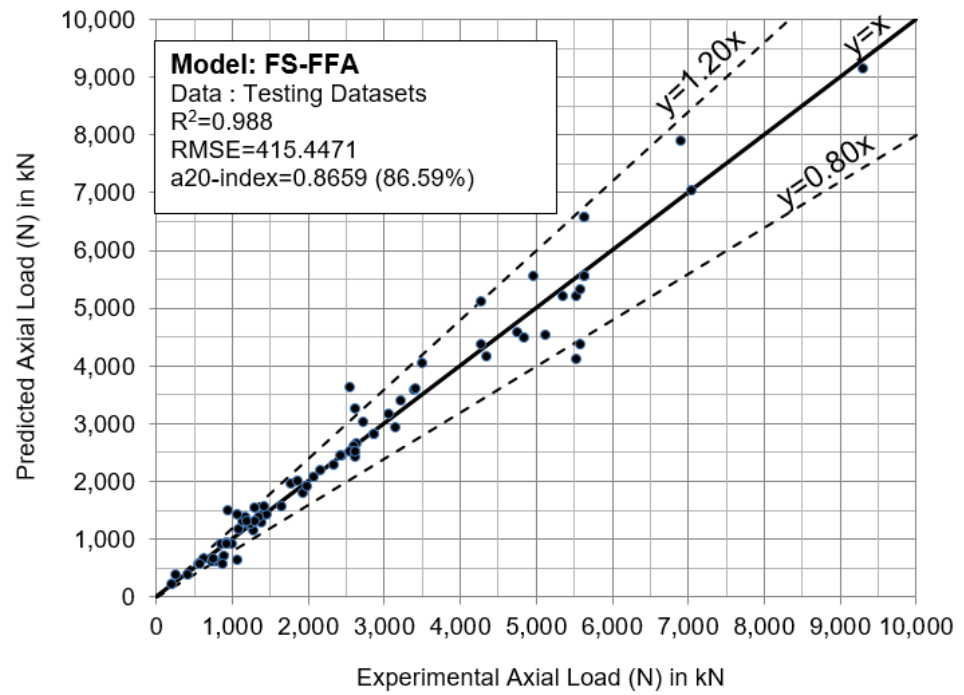
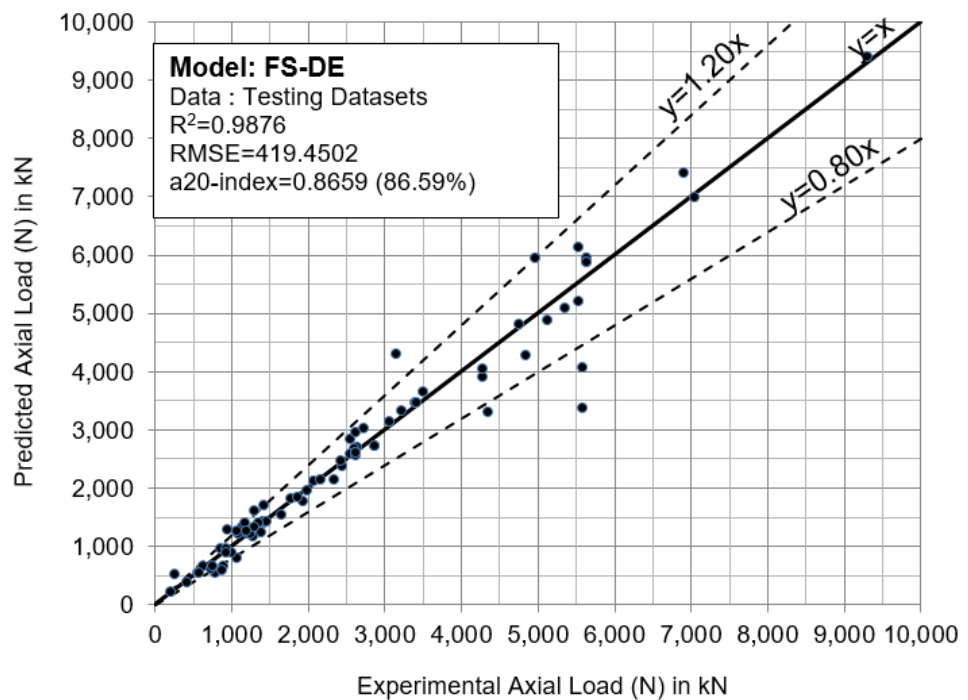


Figure 4. Results of training phase: (a) FS-FFA model, (b) FS-DE model.



(a)



(b)

Figure 5. Results of testing phase: (a) FS-FFA model, (b) FS-DE model.

7. Discussion

7.1. Comparison against Alternative Hybrid Models

In this section, a comparison is made between the developed hybrid models with the base model and the other two traditional hybrid models. Given that optimization algorithms have different performances for each problem, it is possible to identify their differences and compare their performances by examining several algorithms together. Therefore, two hybrid models, FS-genetic algorithm (GA) and FS-particle swarm optimization (PSO), were developed to compare with the two developed models in this study. The findings showed that the FS-FFA, FS-DE, FS-GA, and FS-PSO models outperformed FS in terms of prediction accuracy for training data by 9.68%, 6.58%, 5.68%, and 1.56% respectively. Among the hybrid models, the FS-FFA model provided the best performance according to the various criteria for predicting circular CFST ultimate load values.

7.2. Comparison against Design Codes

In this section a comparison between the two developed models against the predictions of the three design codes, mentioned earlier in the text (EN1994, AISC360 and AIJ) is presented. The design code calculations were performed ignoring any safety factors. Also, the calculations were not focused on the squash load only but took into account the relevant for more slender columns buckling failure methodologies available in each code.

Table 4 presents the performance indices for the two developed models and the respective ones for the design codes. The results correspond to the designated testing datasets among the specimens in the experimental database, amounting to 82 specimens. The various models in the Table are ranked according to their RMSE index. It appears that the two developed models achieve a considerable improvement in almost all indices, compared to the design codes. In particular the improvement from the best performing code which proves the Japanese AIJ [73], is remarkable for both the RMSE and a20-index. A marginal improvement is also found in terms of R^2 index. Among design codes, the AIJ [73] achieves improved performance compared to the other codes.

Table 4. Performance indices on the testing datasets.

Ranking	Model	a20-Index	R^2	RMSE
1	FS-FFA	0.8659	0.9880	415.4471
2	FS-DE	0.8659	0.9876	419.4502
3	AIJ [73]	0.6341	0.9842	786.3858
4	EN1994 [71]	0.5732	0.9681	1119.6477
5	AISC 360 [72]	0.3659	0.9814	1330.6249

Figure 6 illustrates for the two hybrid models and for the examined design codes, the individual experimental vs. predicted load values for all specimens in the testing datasets. It can be visually inspected that the FS-FFA hybrid model achieves a better fit to the experimental values, with less outliers, over the entire range of specimens.

7.3. Limitations and Future Works

This research developed several hybrid models using artificial intelligence to predict the ultimate compressive load of CCFST columns. These models are based on data collected from laboratory works of previous research. Given that the structure of models is highly dependent on the number of parameters, their types must be taken into account in measuring and using such data. Laboratory outline data reduce the accuracy of prediction. On the other hand, the purpose of this study is to develop non-linear models to more accurately evaluate the target parameter. Therefore, a balance between the input data and their statistical characteristics must be elaborated. By doing this, a wider range of data can be analyzed and a model with higher power can be developed. Since these models

have used two optimization algorithms to improve the performance of the base model, some other optimization techniques such as the whale optimization algorithm can be examined to increase the base model performance. The base model in this research was made using the FS model, which has special features, while by changing the basic model to other predictive models such as neuro-fuzzy, new results can be achieved. The last future direction of this research can be related to increasing the number of data samples with circular cross sections to develop a new model with a level of more generalization.

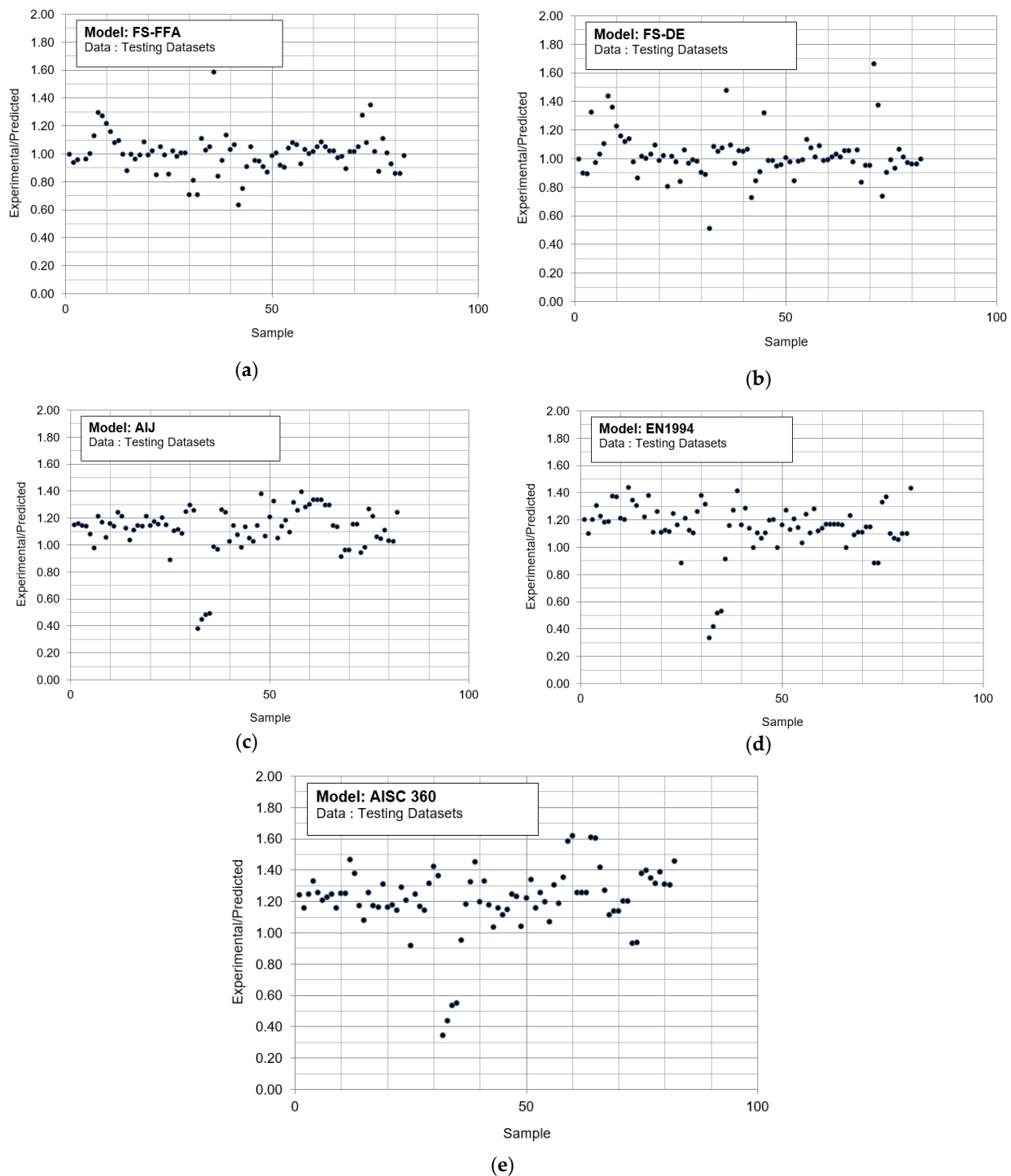


Figure 6. Experimental vs. predicted ratios: (a) the FS-FFA model, (b) the FS-DE model, (c) the AIJ design code model [73], (d) the EN1994 design code model [71], (e) the AISC360 design code model [72].

8. Conclusions

In this study, a novel artificial intelligence-based prediction model is used to correctly evaluate CCFST columns' axial compression capacity. FS and two recent nature meta-heuristic optimization methods known as FFA and DE were combined to create two hybrid FS-FFA and FS-DE models. It was also combined with two common optimization techniques, the GA and PSO. An extensive database of 410 experimental tests for the CCFST columns was gathered from openly available papers for this research project. A statistical and visual analysis was undertaken to determine the effectiveness and correctness of the findings, and the following conclusions can be reached.

According to the research findings, the suggested hybridization models outperformed the basic FS model when it came to resolving the axial compression capacity problem. The findings showed that the FS-FFA, FS-DE, FS-GA, and FS-PSO models outperformed FS in terms of prediction accuracy for training data by 9.68%, 6.58%, 5.68%, and 1.56%, respectively. According to all performance assessments, the new suggested FS-FFA model is optimal for the prediction of the axial compression capacity of CCFTS columns, with improved RMSE and a20-index compared with FS-DE. Additionally, the proposed model achieved a significantly improved prediction of the ultimate compressive load compared to available design code predictions. In particular, RMSE of the FS-FFA model was reduced by 47% from AIJ [73] and more from the EN1994 [71] and AISC360 [72], whereas a20-index was also considerably increased.

The base model in this research was made using the FS model, which has special features, while by changing the basic model to other predictive models such as neuro-fuzzy, new results can be achieved. The last future direction of this research can be related to increasing the number of data samples with circular cross sections to develop a new model with a greater generalization level.

This model's performance and machine learning methods are largely reliant on the database used. However, a more sophisticated and bigger database may have significant effects on the hybrid FS model's final outcomes. Other optimization techniques such as the whale optimization algorithm can be examined to increase the base model performance. Furthermore, other sections' geometries of CFTS, such as squares and round-ended squares, can also be investigated by the proposed hybrid models in this research. Close form equations of this issue using machine learning models will be very beneficial to engineering in the future.

Author Contributions: Conceptualization, P.G.A., M.K., A.S.M. and D.J.A.; Data curation, P.G.A., M.K., A.S.M., M.E.L., A.D.S. and C.M.; Formal analysis, J.L., M.K., A.S.M., L.C., M.Z.T. and A.D.S.; Supervision, P.G.A., A.S.M. and D.J.A.; Writing—original draft, P.G.A., M.K., A.S.M., D.J.A. and J.L.; Writing—review and editing, P.G.A., L.C., M.K., A.S.M., D.J.A., J.L., M.E.L., M.Z.T. and C.M. All authors have read and agreed to the published version of the manuscript.

Funding: This research received no external funding.

Institutional Review Board Statement: Not applicable.

Informed Consent Statement: Not applicable.

Data Availability Statement: The data presented in this study are available in Appendix A.

Conflicts of Interest: The authors confirm that this article content has no conflict of interest.

Nomenclature

DE	differential evolution
D	diameter
HS	harmony search
CFST	concrete-filled steel tubular

CCFST	circular concrete-filled steel tubular
FS	fuzzy systems
FFA	firefly algorithm
fc	the compressive strength
fy	the steel tube yield stress
PSO	particle swarm optimization
L	column length
t	thickness
GA	genetic algorithm
R2	coefficient of determination
RMSE	root mean square error
Pexp	ultimate axial compressive load
Npop	population
ML	machine learning

Appendix A

Table A1. The database used for analysis in this study.

Dataset Number	fc (MPa)	D (mm)	L (mm)	t (mm)	fy (MPa)	Pexp (KN)
1	34.04	60	180	1.48	307	215
2	51.3	101.9	305.7	3.03	371	926
3	34.08	60	180	1.48	307	220
4	164.4	114.3	200	6.3	428	2866
5	103.4	100	300	1.9	404	1100
6	103.4	100	300	1.9	404	1125
7	103.4	100	300	1.9	404	1170
8	51.3	101.5	304.5	3.03	371	859
9	23.1	101.6	304.8	3.03	371	635
10	23.2	101.6	304.8	3.03	371	635
11	40	101.6	304.8	3.03	371	864
12	93.6	114.57	300	3.99	343	1308
13	34.1	101.7	203.3	3.07	605.1	1112.10
14	40	101.7	305.1	3.03	371	803
15	48.3	165	562.5	2.82	363.3	1759
16	23	101.8	305.4	3.03	371	679
17	23.2	101.8	305.4	3.03	371	632
18	40.2	101.6	304.8	3.03	371	864
19	51	101.9	305.7	3.03	371	926
20	34.08	60	180	1.48	307	215
21	25.4	108	324	6.47	853	2275
22	56.99	114.3	342.9	6	342.95	1425.3
23	40.5	108	324	6.47	853	2402
24	43.9	108	1296	4	336	839
25	43.92	108	324	4	336	1235
26	77	108	324	6.47	853	2713
27	40.5	109	327	6.47	853	2446

Table A1. Cont.

Dataset Number	fc (MPa)	D (mm)	L (mm)	t (mm)	fy (MPa)	Pexp (KN)
28	25	114	1250	5.91	486	1177
29	37	114	850	1.79	266	515
30	37	114	850	6	486	1334
31	31.9	114.09	300.5	3.85	343	948
32	97.2	114.26	300	3.93	343	1359
33	57.6	114.29	300	3.75	343	1067
34	31.7	114.3	1143	3.35	287.3	563.6
35	31.7	114.3	342.9	3.35	287.3	816.2
36	31.7	114.3	1143	6	343	909.7
37	31.7	114.3	800.1	6	343	1000.4
38	31.7	114.3	571.5	6	343	1218.7
39	31.75	114.3	342.9	3.35	287.33	816.2
40	31.75	114.3	342.9	6	342.95	1380
41	56.9	114.3	342.9	3.35	287.33	995.7
42	25.4	108	324	6.47	853	2275
43	57	114.3	1143	3.35	287.3	904.2
44	57	114.3	571.5	3.35	287.3	937
45	57	114.3	342.9	3.35	287.3	995.7
46	57	114.3	800.1	6	343	1244.4
47	57	114.3	571.5	6	343	1389.3
48	86.1	114.3	342.9	6	343	1673.9
49	86.2	114.3	1143	3.35	287.3	1200
50	86.2	114.3	571.5	3.35	287.3	1281.4
51	86.2	114.3	1143	6	343	1389.1
52	86.2	114.3	800.1	6	343	1509.3
53	86.2	114.3	571.5	6	343	1564.7
54	86.21	114.3	342.9	3.35	287.33	1242.2
55	86.21	114.3	342.9	6	342.95	1673.9
56	88.8	114.3	342.9	3.35	287.3	1136.20
57	88.8	114.3	571.5	3.35	287.3	1180.70
58	102.4	114.3	1143	3.35	287.3	1481.2
59	102.4	114.3	800.1	3.35	287.3	1513.5
60	102.4	114.3	571.5	3.35	287.3	1598.9
61	102.4	114.3	342.9	3.35	287.3	1610.6
62	102.4	114.3	1143	6	343	1613.5
63	102.4	114.3	800.1	6	343	1788.9
64	102.4	114.3	571.5	6	343	1827.1
65	102.43	114.3	342.9	3.35	287.33	1610.6
66	102.43	114.3	342.9	6	342.95	1943.4
67	107.2	114.3	300	2.74	235	1295.10

Table A1. Cont.

Dataset Number	fc (MPa)	D (mm)	L (mm)	t (mm)	fy (MPa)	Pexp (KN)
68	107.2	114.3	600	5.9	355	1968.10
69	164.35	114.3	200	6.3	428	2595
70	164.35	114.3	200	6.3	428	2866
71	37.5	60	180	1.48	307	215
72	173.5	114.3	250	3.6	403	2340
73	173.5	114.3	250	3.6	403	2422
74	173.5	114.3	250	6.3	403	2610
75	31.4	114.43	300	3.98	343	948
76	57.6	114.49	299.3	3.75	343	1038
77	98.9	114.54	300	3.84	343	1359
78	40.2	101.7	305.1	3.03	371	803
79	34.7	114.88	300.5	4.91	365	1380
80	89.2	115	300	4.92	365	1787
81	57.6	115.02	300.5	5.02	365	1413
82	104.9	115.04	300	4.92	365	1787
83	23.2	101.8	305.4	3.03	371	679
84	34.08	120	360	1.48	307	610
85	34.08	120	360	1.48	307	660
86	36.6	159	650	5	390	2120
87	64.2	159	650	4.8	433	2210
88	56.1	165	581	2.82	363.3	2040
89	110.6	121	370	5	295	2016
90	116.7	121	370	5	295	1996
91	25.4	122	366	4.54	576	1509
92	25.4	122	366	4.54	576	1509
93	40.2	122	366	4.54	576	1657
94	40.5	122	366	4.54	576	1657
95	40.5	122	366	4.54	576	1663
96	40.5	122	366	4.54	576	1663
97	77	122	366	4.54	576	2100
98	77.2	122	366	4.54	576	2100
99	110.6	127.4	390	5.7	295	2217
100	116.7	127.4	390	5.7	295	2266
101	116.7	127.4	390	8.5	295	3106
102	42.1	133	465	2.9	325	476
103	42.1	133	465	4.5	325	492
104	42.1	133	465	4.5	325	576
105	42.2	133	2730	4.5	325	282
106	42.2	133	2730	4.5	325	293
107	42.2	133	1670	4.5	325	335

Table A1. Cont.

Dataset Number	fc (MPa)	D (mm)	L (mm)	t (mm)	fy (MPa)	Pexp (KN)
108	42.2	133	1670	4.5	325	347
109	42.2	133	1670	4.5	325	412
110	42.2	133	1670	4.5	325	430
111	42.2	133	465	2.9	325	466
112	42.2	133	465	2.9	325	476
113	42.2	133	465	4.5	325	500
114	42.2	133	465	4.5	325	559
115	42.2	133	465	4.5	325	576
116	42.2	133	465	4.5	325	591
117	42.2	133	1862	4.5	325	715
118	42.2	133	2793	4.5	325	784
119	42.2	133	2793	4.5	325	800
120	95	133	405	5	295	2002
121	110.6	133	405	5	295	2142
122	116.7	133	405	5	295	2178
123	28.2	140	635	6.68	537	2715
124	52.5	140	420	4.42	1020.00	3020
125	52.5	140	420	8.36	813	4436
126	52.5	140	420	10.46	773	5420
127	125	140	420	6.21	359	3202
128	125	140	420	8.19	389	3354
129	125	140	420	8.19	389	3398
130	125	140	420	11.58	367	4104
131	125	140	420	11.58	367	4300
132	125	140	420	4.42	1020.00	4312
133	125	140	420	4.42	1020.00	4516
134	125	140	420	16.72	389	5120
135	125	140	420	6.27	1153.00	5386
136	125	140	420	8.36	813	5502
137	125	140	420	10.46	773	6187
138	125	140	420	10.46	773	6339
139	40.5	149	447	2.96	308	1080
140	77	149	447	2.96	308	1781
141	77.1	149	447	2.96	308	1781
142	95	152	465	5.5	295	2662
143	116.7	152	465	5.5	295	2851
144	170	152.4	942.9	8.8	392.6	3919.9
145	170	152.4	551.9	8.8	392.6	4200.8
146	178.4	152.4	940.2	6.3	373.4	3584.7
147	178.4	152.4	552.7	6.3	373.4	4033

Table A1. Cont.

Dataset Number	fc (MPa)	D (mm)	L (mm)	t (mm)	fy (MPa)	Pexp (KN)
148	178.8	152.4	943.8	8.8	392.6	4099.8
149	180.9	152.4	949.7	5	445.9	3383.4
150	182.8	152.4	950.5	5	445.9	3995.7
151	182.8	152.4	540.7	5	445.9	4224
152	185.7	152.4	947.3	6.3	373.4	3535.3
153	185.7	152.4	554.7	6.3	373.4	3808
154	185.7	152.4	951.3	8.8	392.6	4178.7
155	185.7	152.4	559.7	8.8	392.6	4288.5
156	185.8	152.4	951.3	5	445.9	3724.1
157	185.8	152.4	548.5	5	445.9	3997.5
158	188.1	152.4	553	6.3	373.4	3692.8
159	188.1	152.4	948.5	6.3	373.4	3861.1
160	42	152.6	304.9	4.93	633.4	2909.10
161	43.4	152.6	304.9	4.9	633.4	2913.60
162	37.5	120	360	1.48	307	660
163	36.6	159	650	6.8	402	2830
164	36.6	159	650	10	355	3400
165	64.1	159	650	4.8	433	2210
166	38	165	571	2.82	363.3	1649
167	37.5	120	360	1.48	307	660
168	48.3	190	658	1.52	306.1	1841
169	48.2	165	562.5	2.82	363.3	1759
170	64.5	159	650	4.8	433	2240
171	93.6	159	650	5	390	2970
172	93.6	159	650	10	355	3400
173	93.8	159	650	5	390	2970
174	93.8	159	650	6.8	402	3410
175	106	159.6	3500	4.98	270	1454
176	71	159.7	2500	5.2	281	1562
177	101	159.7	3000	4.97	275	1636
178	70	159.8	2000	5.01	283	1650
179	73	159.8	3000	5.1	276	1468
180	100	159.8	2500	5.01	275	1818
181	102	159.8	4000	4.97	270	1333
182	45	159.9	4000	4.98	281	1091
183	40	160.1	2000	4.98	280	1261
184	74	160.1	3500	4.98	276	1326
185	100	160.1	200	4.99	275	2550
186	41	160.2	2500	4.96	281	1244
187	71	160.2	4000	5.02	281	1231

Table A1. Cont.

Dataset Number	fc (MPa)	D (mm)	L (mm)	t (mm)	fy (MPa)	Pexp (KN)
188	43	160.3	3000	5	270	1236
189	99	160.3	2000	5.03	281	2000
190	158.46	164.2	652	2.5	377	3501
191	64.3	159	650	4.8	433	2210
192	38.1	165	571	2.82	363.3	1649
193	64.2	159	650	4.8	433	2240
194	48.1	165	562.5	2.82	363.3	1759
195	38.1	190	657	1.13	185.7	1308
196	37.5	120	360	1.48	307	610
197	34	120	360	1.48	307	660
198	95.8	168.6	645	3.9	363	3339
199	56.4	165	581	2.82	363.3	2040
200	67.9	165	500	2.76	350	2250
201	67.94	165	500	2.81	350	2160
202	67.94	165	500	2.76	350	2250
203	77	165	571	1.82	363.3	2608
204	34.08	180	540	1.48	307	1280
205	80.2	165	580.5	2.82	363.3	2295
206	108	165	577.5	2.82	363.3	2673
207	74.7	190	663.5	0.86	210.7	2451
208	29.5	165.2	200	3.7	366	1630.56
209	43.5	165.2	200	3.7	366	1676.42
210	43.5	165.2	200	3.7	366	1737.94
211	58	165.2	200	3.7	366	2094.15
212	58	165.2	200	3.7	366	2221.62
213	81.6	165.2	200	3.7	366	2511.3
214	81.6	165.2	200	3.7	366	2922.24
215	158.7	168.1	645	8.1	409	5254
216	48.2	190	658	1.52	306.1	1841
217	36.2	168.6	645	3.9	363	1771
218	56.3	165	581	2.82	363.3	2040
219	95.8	168.6	645	3.9	363	3339
220	165.49	168.6	648	3.9	363	4216
221	77.1	190	664	0.86	210.7	2553
222	158.75	168.7	645	5.2	405	4751
223	151.9	168.8	650	5.7	452	4930
224	56.4	190	664.5	0.86	210.7	1940
225	167.87	169	645	4.8	399	4330
226	38.2	165	571	2.82	363.3	1649
227	34	180	540	1.48	307	1280

Table A1. Cont.

Dataset Number	fc (MPa)	D (mm)	L (mm)	t (mm)	fy (MPa)	Pexp (KN)
228	38.2	216.5	649.5	6.61	452	4200
229	34.08	180	540	1.48	307	1311
230	37.2	180	540	1.48	307	1280
231	64.4	159	650	4.8	433	2210
232	37.5	180	540	1.48	307	1311
233	158.46	189	756	3	398	4837
234	38	190	657.5	0.86	210.7	1240
235	38	190	657	1.13	185.7	1308
236	38.1	190	657.5	0.86	210.7	1240
237	108	190	660	1.94	256.4	3360
238	38.1	190	659.5	1.94	256.4	1652
239	38.2	190	657.5	0.86	210.7	1240
240	41.1	300	900	2.96	279	3277
241	77.1	165	571	2.82	363.3	2608
242	48.1	190	658	1.52	306.1	1841
243	151.91	168.8	650	5.7	452	4930
244	77.2	190	656	1.94	256.4	3083
245	56.1	190	664.5	0.86	210.7	1940
246	56.2	190	661.5	1.13	185.7	1862
247	56.2	190	664.5	0.86	210.7	1940
248	56.2	190	655.5	1.94	256.4	2338
249	56.4	190	661.5	1.13	185.7	1862
250	165.5	168.6	648	3.9	363	4216
251	37.5	180	540	1.48	307	1280
252	74.2	190	657.5	0.86	210.7	2433
253	113.5	190	660	2	271.9	3360
254	113.5	165	577.5	3	364.3	2673
255	74.7	190	663.5	1.94	256.4	2592
256	77	190	664	0.86	210.7	2553
257	77	190	658	1.52	306.1	2830
258	77	222	666	6.47	843	7304
259	167.9	169	645	4.8	399	4330
260	77.1	190	658	1.52	306.1	2830
261	77.1	190	656	1.94	256.4	3083
262	39.2	318.4	955.2	10.37	335	7742
263	24.3	216.5	649.5	6.61	452	3568
264	80.1	190	662.5	1.13	185.7	2295
265	80.2	190	663.5	1.52	306.1	2602
266	80.2	190	658.5	1.52	306.1	2870
267	85.1	450	1350.00	2.96	279	11,665

Table A1. Cont.

Dataset Number	fc (MPa)	D (mm)	L (mm)	t (mm)	fy (MPa)	Pexp (KN)
268	108	190	661	1.13	185.7	3220
269	108	190	661.5	1.52	306.1	3260
270	38.2	190	659.5	1.94	256.4	1652
271	108.1	190	661.5	1.13	185.7	3220
272	40.5	222	666	6.47	843	5714
273	113.5	190	660	1.15	184.8	3058
274	113.5	190	662	0.95	211.2	3070
275	113.5	190	661.5	1.55	315.3	3260
276	25.4	337	1011.00	6.47	823	8475
277	46.7	216.4	649.2	6.61	452	4283
278	24.1	216.5	649.5	6.61	452	3568
279	56.4	190	655.5	1.94	256.4	2338
280	38.1	216.5	649.5	6.61	452	4200
281	41.1	337	1011	6.47	823	9835
282	108	219	708	6.3	300	5410
283	148.8	219.1	600	6.3	300	6838
284	163	219.1	600	6.3	300	6915
285	174.5	219.1	600	6.3	300	7569
286	175.4	219.1	600	6.3	300	7407
287	185.1	219.1	600	5	380	7837
288	185.1	219.1	600	10	381	9085
289	25.4	222	666	6.47	843	4964
290	108.2	190	661	1.13	185.7	3220
291	26.9	550	1000.00	16	546	28,830
292	77	222	666	6.47	843	7304
293	77.2	190	658	1.52	306.1	2830
294	40.5	238	714	4.54	507	3583
295	40.5	238	714	4.54	507	3647
296	25.4	239	717	4.54	507	3035
297	74.7	190	657.5	0.86	210.7	2433
298	34.08	240	720	1.48	307	2150
299	34.08	240	720	1.48	307	2300
300	41.1	337	1011.00	6.47	823	9668
301	37.5	240	720	1.48	307	2150
302	41.1	361	1083	4.54	525	7260
303	38.2	190	657	1.13	185.7	1308
304	25.4	301	903	2.96	279	2382
305	80.3	301	903	2.96	279	5540
306	52.2	318.3	954.9	10.37	335	9297
307	39.1	318.4	955.2	10.37	335	7742

Table A1. Cont.

Dataset Number	fc (MPa)	D (mm)	L (mm)	t (mm)	fy (MPa)	Pexp (KN)
308	77	190	656	1.94	256.4	3083
309	24.2	318.5	955.5	10.37	335	6901
310	92.3	323.9	1000.00	5.6	443.9	11,481
311	25.4	337	1011	6.47	823	8475
312	34.01	240	720	1.48	307	2300
313	41.1	337	1011	6.47	823	9668
314	158.75	168.1	645	8.1	409	5254
315	37.5	240	720	1.48	307	2300
316	41.1	337	1011.00	6.47	823	9835
317	85.1	337	1011	6.47	823	13,776
318	41.1	360	1080	4.54	525	7045
319	85.1	360	1080	4.54	525	11,505
320	37.2	240	720	1.48	307	2300
321	41.1	361	1083.00	4.54	525	7260
322	25.4	450	1350	2.96	279	4415
323	41.1	450	1350	2.96	279	6870
324	41.1	450	1350	2.96	279	6985
325	85.1	450	1350	2.96	279	11,665
326	108	190	660	1.13	185.7	3058
327	40.5	222	666	6.47	843	5714
328	26.9	550	1000.00	16	546	29,590
329	37.5	60	180	1.48	307	215
330	103.4	100	300	1.9	404	1085.00
331	51.3	101.5	304.5	3.03	371	859
332	33.9	101.7	203.3	3.07	605.1	1067.60
333	23.2	101.8	305.4	3.03	371	632
334	40.5	109	327	6.47	853	2446
335	25	114	1280	5.94	486	1285
336	37	114	850	3.35	291	785
337	37	114	850	4.44	332	902
338	31.7	114.3	800.1	3.35	287.3	736.8
339	31.7	114.3	571.5	3.35	287.3	749.4
340	31.7	114.3	342.9	6	343	1380
341	31.9	114.3	300	3.85	343	998
342	57	114.3	800.1	3.35	287.3	932.9
343	57	114.3	1143	6	343	1141.3
344	57	114.3	342.9	6	343	1425.3
345	86.2	114.3	800.1	3.35	287.3	1206.5
346	86.2	114.3	342.9	3.35	287.3	1242.2
347	102.4	114.3	342.9	6	343	1943.4

Table A1. Cont.

Dataset Number	fc (MPa)	D (mm)	L (mm)	t (mm)	fy (MPa)	Pexp (KN)
348	105.5	114.3	571.5	3.35	287.3	1407.10
349	105.5	114.3	342.9	3.35	287.3	1453.10
350	107.2	114.3	600	2.74	235	1296.60
351	107.2	114.3	300	5.9	355	1989.90
352	173.5	114.3	250	6.3	403	2633
353	98.9	114.37	299.5	3.85	343	1182
354	34.7	114.43	300	3.82	343	929
355	84.1	114.5	300	3.84	343	1359
356	79.6	114.6	300	3.99	343	1308
357	77.1	190	662	1.13	185.7	2630
358	95	127.4	390	8.5	295	2544
359	110.6	127.4	390	8.5	295	2623
360	42.2	133	2730	4.5	325	268
361	42.2	133	1670	4.5	325	416
362	42.2	133	465	4.5	325	568
363	42.2	133	465	4.5	325	582
364	42.2	133	1862	4.5	325	882
365	52.5	140	420	6.27	1153.00	4274
366	125	140	420	6.21	359	3215
367	125	140	420	16.72	389	5135
368	125	140	420	6.27	1153.00	5354
369	95	127.4	390	5.7	295	2078
370	25.4	149	447	2.96	308	941
371	40.5	149	447	2.96	308	1064
372	110.6	152	465	5.5	295	2734
373	178.8	152.4	549.8	8.8	392.6	4354.1
374	93.8	159	650	10	355	3400
375	77.1	190	662.5	1.13	185.7	2630
376	80	190	658.5	1.52	306.1	2870
377	158.5	164.2	652	2.5	377	3501
378	67.9	165	500	2.81	350	2160
379	41	160.2	3500	4.97	273	1193
380	29.5	165.2	200	3.7	366	1428.32
381	36.2	168.6	645	3.9	363	1771
382	158.7	168.7	645	5.2	405	4751
383	158.5	189	756	3	398	4837
384	38.2	190	659.5	1.94	256.4	1652
385	56.4	190	661.5	1.13	185.7	1862
386	56.4	190	655.5	1.94	256.4	2338
387	74.7	190	657.5	0.86	210.7	2433

Table A1. Cont.

Dataset Number	fc (MPa)	D (mm)	L (mm)	t (mm)	fy (MPa)	Pexp (KN)
388	77.1	190	664	0.86	210.7	2553
389	93.8	159	650	6.8	402	3410
390	125	140	420	8.36	813	5531
391	77.1	190	662	1.13	185.7	2630
392	77	165	571	2.82	363.3	2608
393	80.2	190	658.5	1.52	306.1	2870
394	108	190	662	0.86	210.7	3070
395	46.7	216.4	649.2	6.61	452	4283
396	25.4	222	666	6.47	843	4964
397	40.4	222	666	6.47	843	5638
398	40.5	222	666	6.47	843	5638
399	77	238	714	4.54	507	5578
400	77	238	714	4.54	507	5578
401	41.1	300	900	2.96	279	3152
402	80.3	301	903	2.96	279	5540
403	52.2	318.3	954.9	10.37	335	9297
404	24.2	318.5	955.5	10.37	335	6901
405	85.1	337	1011.00	6.47	823	13,776
406	41.1	360	1080.00	4.54	525	7045
407	85.1	360	1080.00	4.54	525	11,505
408	25.2	361	1083.00	4.54	525	5633
409	25.4	361	1083	4.54	525	5633
410	26.9	550	1000.00	16	546	29,050

References

- Wang, F.; Han, L.; Li, W. Analytical behavior of CFDST stub columns with external stainless steel tubes under axial compression. *Thin-Walled Struct.* **2018**, *127*, 756–768. [CrossRef]
- Design, A.S. Specification for structural steel buildings. *AISC Dec.* **1999**, *27*, 1–210.
- Nishiyama, I. *Summary of Research on Concrete-Filled Structural Steel Tube Column System Carried out under the US-Japan Cooperative Research Program on Composite and Hybrid Structures*; Building Research Institution: Uttarakhand, India, 2002.
- Kim, D.K. A Database for Composite Columns. 2005. Available online: <http://hdl.handle.net/1853/7126> (accessed on 20 May 2005).
- Han, L.H. *Concrete Filled Steel Tube Structures-Theory and Application*; Science Press: Beijing, China, 2007.
- Cederwall, K.; Engstrom, B.; Grauers, M. High-strength concrete used in composite columns. *Spec. Publ.* **1990**, *121*, 195–214.
- Varma, A.H. *Seismic Behavior, Analysis, and Design of High Strength Square Concrete Filled Steel Tube (CFT) Columns*; Lehigh University: Bethlehem, PA, USA, 2001.
- Uy, B. Strength of short concrete filled high strength steel box columns. *J. Constr. Steel Res.* **2001**, *57*, 113–134. [CrossRef]
- Liu, D.; Gho, W.-M.; Yuan, J. Ultimate capacity of high-strength rectangular concrete-filled steel hollow section stub columns. *J. Constr. Steel Res.* **2003**, *59*, 1499–1515. [CrossRef]
- Mursi, M.; Uy, B. Strength of slender concrete filled high strength steel box columns. *J. Constr. Steel Res.* **2004**, *60*, 1825–1848. [CrossRef]
- Sakino, K.; Nakahara, H.; Morino, S.; Nishiyama, I. Behavior of centrally loaded concrete-filled steel-tube short columns. *J. Struct. Eng.* **2004**, *130*, 180–188. [CrossRef]
- Lue, D.M.; Liu, J.-L.; Yen, T. Experimental study on rectangular CFT columns with high-strength concrete. *J. Constr. Steel Res.* **2007**, *63*, 37–44. [CrossRef]
- Aslani, F.; Uy, B.; Tao, Z.; Mashiri, F. Behaviour and design of composite columns incorporating compact high-strength steel plates. *J. Constr. Steel Res.* **2015**, *107*, 94–110. [CrossRef]

14. Xiong, M.-X.; Xiong, D.-X.; Liew, J.Y.R. Axial performance of short concrete filled steel tubes with high-and ultra-high-strength materials. *Eng. Struct.* **2017**, *136*, 494–510. [[CrossRef](#)]
15. Lai, Z.; Varma, A.H. High-strength rectangular CFT members: Database, modeling, and design of short columns. *J. Struct. Eng.* **2018**, *144*, 4018036. [[CrossRef](#)]
16. Gardner, N.J.; Jacobson, E.R. Structural behavior of concrete filled steel tubes. *J. Proc.* **1967**, *64*, 404–413.
17. Bergmann, R. Load introduction in composite columns filled with high strength concrete. In *Tubular Structures VI*; Routledge: Oxfordshire, UK, 2021; pp. 373–380.
18. O'Shea, M.D.; Bridge, R.Q. Circular thin-walled tubes with high strength concrete infill. In Proceedings of the Composite Construction in Steel and Concrete III, New York, NY, USA, 9–14 June 1996; pp. 780–793.
19. Schneider, S.P. Axially loaded concrete-filled steel tubes. *J. Struct. Eng.* **1998**, *124*, 1125–1138. [[CrossRef](#)]
20. O'Shea, M.D.; Bridge, R.Q. Design of circular thin-walled concrete filled steel tubes. *J. Struct. Eng.* **2000**, *126*, 1295–1303. [[CrossRef](#)]
21. Giakoumelis, G.; Lam, D. Axial capacity of circular concrete-filled tube columns. *J. Constr. Steel Res.* **2004**, *60*, 1049–1068. [[CrossRef](#)]
22. Zeghiche, J.; Chaoui, K. An experimental behaviour of concrete-filled steel tubular columns. *J. Constr. Steel Res.* **2005**, *61*, 53–66. [[CrossRef](#)]
23. Yu, Q.; Tao, Z.; Wu, Y.-X. Experimental behaviour of high performance concrete-filled steel tubular columns. *Thin-Walled Struct.* **2008**, *46*, 362–370. [[CrossRef](#)]
24. de Oliveira, W.L.A.; De Nardin, S.; de Cresce El, A.L.H.; El Debs, M.K. Influence of concrete strength and length/diameter on the axial capacity of CFT columns. *J. Constr. Steel Res.* **2009**, *65*, 2103–2110. [[CrossRef](#)]
25. Liew, J.Y.R.; Xiong, D.X. Effect of preload on the axial capacity of concrete-filled composite columns. *J. Constr. Steel Res.* **2009**, *65*, 709–722. [[CrossRef](#)]
26. Chen, G.; Xu, Z.; Yang, Z.; Tian, Z. Experimental study on behavior of short steel tubular columns filled with ultra-high strength concrete mixed with stone-chip subjected to axial load. *J. Build. Struct.* **2011**, *32*, 82–89.
27. Tang, D.; Gordan, B.; Koopialipoor, M.; Jahed Armaghani, D.; Tarinejad, R.; Thai Pham, B.; Huynh, V. Van seepage analysis in short embankments using developing a metaheuristic method based on governing equations. *Appl. Sci.* **2020**, *10*, 1761. [[CrossRef](#)]
28. Ye, J.; Koopialipoor, M.; Zhou, J.; Armaghani, D.J.; He, X. A novel combination of tree-based modeling and monte carlo simulation for assessing risk levels of flyrock induced by mine blasting. *Nat. Resour. Res.* **2020**, *30*, 225–243. [[CrossRef](#)]
29. Yang, H.; Wang, Z.; Song, K. A new hybrid grey wolf optimizer-feature weighted-multiple kernel-support vector regression technique to predict TBM performance. *Eng. Comput.* **2020**, 1–17. [[CrossRef](#)]
30. Zhou, J.; Chen, C.; Wang, M.; Khandelwal, M. Proposing a novel comprehensive evaluation model for the coal burst liability in underground coal mines considering uncertainty factors. *Int. J. Min. Sci. Technol.* **2021**, *31*, 799–812. [[CrossRef](#)]
31. Zhou, J.; Qiu, Y.; Khandelwal, M.; Zhu, S.; Zhang, X. Developing a hybrid model of Jaya algorithm-based extreme gradient boosting machine to estimate blast-induced ground vibrations. *Int. J. Rock Mech. Min. Sci.* **2021**, *145*, 104856. [[CrossRef](#)]
32. Zhou, J.; Li, X.; Mitri, H.S. Classification of rockburst in underground projects: Comparison of ten supervised learning methods. *J. Comput. Civ. Eng.* **2016**, *30*, 4016003. [[CrossRef](#)]
33. Asteris, P.G.; Cavaleri, L.; Ly, H.-B.; Pham, B.T. Surrogate models for the compressive strength mapping of cement mortar materials. *Soft Comput.* **2021**, *25*, 6347–6372. [[CrossRef](#)]
34. Harandizadeh, H.; Armaghani, D.; Asteris Panagiotis, G.; Gandomi, A.H. TBM performance prediction developing a hybrid ANFIS-PNN predictive model optimized by imperialism competitive algorithm. *Neural. Comput. Appl.* **2021**, *33*, 16149–16179. [[CrossRef](#)]
35. Mohammed, A.S.; Asteris, P.G.; Koopialipoor, M.; Alexakis, D.E.; Lemonis, M.E.; Armaghani, D.J. Stacking ensemble tree models to predict energy performance in residential buildings. *Sustainability* **2021**, *13*, 8298. [[CrossRef](#)]
36. Armaghani, D.J.; Mamou, A.; Maraveas, C.; Roussis, P.C.; Siorikis, V.G.; Skentou, A.D.; Asteris, P.G. Predicting the unconfined compressive strength of granite using only two non-destructive test indexes. *Geomech. Eng.* **2021**, *25*, 317–330.
37. Ke, B.; Khandelwal, M.; Asteris, P.G.; Skentou, A.D.; Mamou, A.; Armaghani, D.J. Rock-burst occurrence prediction based on optimized Naïve Bayes models. *IEEE Access.* **2021**, *9*, 91347–91360. [[CrossRef](#)]
38. Asteris, P.G.; Lourenço, P.B.; Hajihassani, M.; Adami, C.-E.N.; Lemonis, M.E.; Skentou, A.D.; Marques, R.; Nguyen, H.; Rodrigues, H.; Varum, H. Soft computing-based models for the prediction of masonry compressive strength. *Eng. Struct.* **2021**, *248*, 113276. [[CrossRef](#)]
39. Yang, H.; Koopialipoor, M.; Armaghani, D.J.; Gordan, B.; Khorami, M.; Tahir, M.M. Intelligent design of retaining wall structures under dynamic conditions. *STEEL Compos. Struct.* **2019**, *31*, 629–640.
40. Asteris, P.G.; Lemonis, M.E.; Le, T.-T.; Tsavdaridis, K.D. Evaluation of the ultimate eccentric load of rectangular CFSTs using advanced neural network modeling. *Eng. Struct.* **2021**, *248*, 113297. [[CrossRef](#)]
41. Nguyen, N.-H.; Vo, T.P.; Lee, S.; Asteris, P.G. Heuristic algorithm-based semi-empirical formulas for estimating the compressive strength of the normal and high performance concrete. *Constr. Build. Mater.* **2021**, *304*, 124467. [[CrossRef](#)]
42. Asteris, P.G.; Lemonis, M.E.; Nguyen, T.-A.; Van Le, H.; Pham, B.T. Soft computing-based estimation of ultimate axial load of rectangular concrete-filled steel tubes. *Steel Compos. Struct.* **2021**, *39*, 471.
43. Colesanti, C.; Wasowski, J. Investigating landslides with space-borne Synthetic Aperture Radar (SAR) interferometry. *Eng. Geol.* **2006**, *88*, 173–199. [[CrossRef](#)]

44. Asteris, P.G.; Skentou, A.D.; Bardhan, A.; Samui, P.; Lourenço, P.B. Soft computing techniques for the prediction of concrete compressive strength using Non-Destructive tests. *Constr. Build. Mater.* **2021**, *303*, 124450. [[CrossRef](#)]
45. Asteris, P.G.; Skentou, A.D.; Bardhan, A.; Samui, P.; Pilakoutas, K. Predicting concrete compressive strength using hybrid ensembling of surrogate machine learning models. *Cem. Concr. Res.* **2021**, *145*, 106449. [[CrossRef](#)]
46. Bardhan, A.; Gokceoglu, C.; Burman, A.; Samui, P.; Asteris, P.G. Efficient computational techniques for predicting the California bearing ratio of soil in soaked conditions. *Eng. Geol.* **2021**, *291*, 106239. [[CrossRef](#)]
47. Parsajoo, M.; Armaghani, D.J.; Mohammed, A.S.; Khari, M.; Jahandari, S. Tensile strength prediction of rock material using non-destructive tests: A comparative intelligent study. *Transp. Geotech.* **2021**, *31*, 100652. [[CrossRef](#)]
48. Parsajoo, M.; Armaghani, D.J.; Asteris, P.G. A precise neuro-fuzzy model enhanced by artificial bee colony techniques for assessment of rock brittleness index. *Neural. Comput. Appl.* **2021**, 1–19. [[CrossRef](#)]
49. Pham, B.T.; Nguyen, M.D.; Nguyen-Thoi, T.; Ho, L.S.; Koopialipoor, M.; Quoc, N.K.; Armaghani, D.J.; Van Le, H. A novel approach for classification of soils based on laboratory tests using Adaboost, Tree and ANN modeling. *Transp. Geotech.* **2020**, *27*, 100508. [[CrossRef](#)]
50. Mohamad, E.T.; Koopialipoor, M.; Murlidhar, B.R.; Rashidell, A.; Hedayat, A.; Armaghani, D.J. A new hybrid method for predicting ripping production in different weathering zones through in-situ tests. *Measurement* **2019**, *147*, 106826. [[CrossRef](#)]
51. Cai, M.; Koopialipoor, M.; Armaghani, D.J.; Thai Pham, B. Evaluating slope deformation of earth dams due to earthquake shaking using MARS and GMDH techniques. *Appl. Sci.* **2020**, *10*, 1486. [[CrossRef](#)]
52. Huang, J.; Koopialipoor, M.; Armaghani, D.J. A combination of fuzzy Delphi method and hybrid ANN-based systems to forecast ground vibration resulting from blasting. *Sci. Rep.* **2020**, *10*, 1–21. [[CrossRef](#)] [[PubMed](#)]
53. Guo, H.; Zhou, J.; Koopialipoor, M.; Armaghani, D.J.; Tahir, M.M. Deep neural network and whale optimization algorithm to assess flyrock induced by blasting. *Eng. Comput.* **2019**, *37*, 173–186. [[CrossRef](#)]
54. Xu, C.; Gordan, B.; Koopialipoor, M.; Armaghani, D.J.; Tahir, M.M.; Zhang, X. Improving performance of retaining walls under dynamic conditions developing an optimized ANN based on ant colony optimization technique. *IEEE Access* **2019**, *7*, 94692–94700. [[CrossRef](#)]
55. Yang, H.Q.; Xing, S.G.; Wang, Q.; Li, Z. Model test on the entrainment phenomenon and energy conversion mechanism of flow-like landslides. *Eng. Geol.* **2018**, *239*, 119–125. [[CrossRef](#)]
56. Huang, L.; Asteris, P.G.; Koopialipoor, M.; Armaghani, D.J.; Tahir, M.M. Invasive weed optimization technique-based ANN to the prediction of rock tensile strength. *Appl. Sci.* **2019**, *9*, 5372. [[CrossRef](#)]
57. Lu, S.; Koopialipoor, M.; Asteris, P.G.; Bahri, M.; Armaghani, D.J. A novel feature selection approach based on tree models for evaluating the punching shear capacity of steel fiber-reinforced concrete flat slabs. *Materials* **2020**, *13*, 3902. [[CrossRef](#)]
58. Asteris, P.G.; Koopialipoor, M.; Armaghani, D.J.; Kotsonis, E.A.; Lourenço, P.B. Prediction of cement-based mortars compressive strength using machine learning techniques. *Neural Comput. Appl.* **2021**, *33*, 13089–13121. [[CrossRef](#)]
59. Gao, J.; Koopialipoor, M.; Armaghani, D.J.; Ghabussi, A.; Baharom, S.; Morasaei, A.; Shariati, A.; Khorami, M.; Zhou, J. Evaluating the bond strength of FRP in concrete samples using machine learning methods. *Smart Struct. Syst.* **2020**, *26*, 403–418.
60. Sarir, P.; Chen, J.; Asteris, P.G.; Armaghani, D.J.; Tahir, M.M. Developing GEP tree-based, neuro-swarm, and whale optimization models for evaluation of bearing capacity of concrete-filled steel tube columns. *Eng. Comput.* **2019**, *37*, 1–19. [[CrossRef](#)]
61. Ahmadi, M.; Naderpour, H.; Kheyroddin, A. ANN model for predicting the compressive strength of circular steel-confined concrete. *Int. J. Civ. Eng.* **2017**, *15*, 213–221. [[CrossRef](#)]
62. Ahmadi, M.; Naderpour, H.; Kheyroddin, A. Utilization of artificial neural networks to prediction of the capacity of CCFT short columns subject to short term axial load. *Arch. Civ. Mech. Eng.* **2014**, *14*, 510–517. [[CrossRef](#)]
63. Güneysi, E.M.; Gültekin, A.; Mermerdaş, K. Ultimate capacity prediction of axially loaded CFST short columns. *Int. J. Steel Struct.* **2016**, *16*, 99–114. [[CrossRef](#)]
64. Ipek, S.; Güneysi, E.M. Ultimate axial strength of concrete-filled double skin steel tubular column sections. *Adv. Civ. Eng.* **2019**, *2019*. [[CrossRef](#)]
65. Moon, J.; Kim, J.J.; Lee, T.-H.; Lee, H.-E. Prediction of axial load capacity of stub circular concrete-filled steel tube using fuzzy logic. *J. Constr. Steel Res.* **2014**, *101*, 184–191. [[CrossRef](#)]
66. Al-Khaleefi, A.M.; Terro, M.J.; Alex, A.P.; Wang, Y. Prediction of fire resistance of concrete filled tubular steel columns using neural networks. *Fire Saf. J.* **2002**, *37*, 339–352. [[CrossRef](#)]
67. Ren, Q.; Li, M.; Zhang, M.; Shen, Y.; Si, W. Prediction of ultimate axial capacity of square concrete-filled steel tubular short columns using a hybrid intelligent algorithm. *Appl. Sci.* **2019**, *9*, 2802. [[CrossRef](#)]
68. Tran, V.-L.; Thai, D.-K.; Kim, S.-E. Application of ANN in predicting ACC of SCFST column. *Compos. Struct.* **2019**, *228*, 111332. [[CrossRef](#)]
69. Lee, S.; Vo, T.P.; Thai, H.-T.; Lee, J.; Patel, V. Strength prediction of concrete-filled steel tubular columns using Categorical Gradient Boosting algorithm. *Eng. Struct.* **2021**, *238*, 112109. [[CrossRef](#)]
70. Zarringol, M.; Thai, H.-T.; Thai, S.; Patel, V. Application of ANN to the design of CFST columns. *Structures* **2020**, *28*, 2203–2220. [[CrossRef](#)]
71. The European Union. *European C. for Design of Composite Steel and Concrete Structures*; CEN: Salt Lake City, UT, USA, 1994.
72. Committee, A. *Specification for Structural Steel Buildings*; ANSI/AISC 360-10; American Institute of Steel Construction: Chicago, IL, USA, 22 June 2010.

73. AIJ. Recommendations for design and construction of concrete filled steel tubular structures. *Open J. Civ. Eng.* **1997**, *3*, 3.
74. Zadeh, L.A. A fuzzy-algorithmic approach to the definition of complex or imprecise concepts. *Int. J. Man. Mach. Stud.* **1976**, *8*, 249–291. [[CrossRef](#)]
75. Wang, L.-X. *A Course in Fuzzy Systems*; Prentice-Hall International, Inc.: Hoboken, NJ, USA, 1999.
76. Ali, M.M.; Khompatraporn, C.; Zabinsky, Z.B. A numerical evaluation of several stochastic algorithms on selected continuous global optimization test problems. *J. Glob. Optim.* **2005**, *31*, 635–672. [[CrossRef](#)]
77. Yang, X.-S. Firefly algorithm, stochastic test functions and design optimisation. *Int. J. Bio-Inspired Comput.* **2010**, *2*, 78–84. [[CrossRef](#)]
78. Kaur, M.; Ghosh, S. Network reconfiguration of unbalanced distribution networks using fuzzy-firefly algorithm. *Appl. Soft Comput.* **2016**, *49*, 868–886. [[CrossRef](#)]
79. Zhang, Y.; Wu, L. A novel method for rigid image registration based on firefly algorithm. *Int. J. Res. Rev. Soft Intell. Comput.* **2012**, *2*, 141–146.
80. Apostolopoulos, T.; Vlachos, A. Application of the firefly algorithm for solving the economic emissions load dispatch problem. *Int. J. Comb.* **2010**, *2011*. [[CrossRef](#)]
81. Koopialipoor, M.; Fahimifar, A.; Ghaleini, E.N.; Momenzadeh, M.; Armaghani, D.J. Development of a new hybrid ANN for solving a geotechnical problem related to tunnel boring machine performance. *Eng. Comput.* **2019**, *36*, 345–357. [[CrossRef](#)]
82. Koopialipoor, M.; Noorbakhsh, A.; Noroozi Ghaleini, E.; Jahed Armaghani, D.; Yagiz, S. A new approach for estimation of rock brittleness based on non-destructive tests. *Nondestruct. Test. Eval.* **2019**, *34*, 354–375. [[CrossRef](#)]
83. Gholizadeh, S.; Barati, H. A comparative study of three metaheuristics for optimum design of trusses. *Int. J. Optim. Civ. Eng.* **2012**, *2*, 3.
84. Hancer, E.; Xue, B.; Zhang, M. Differential evolution for filter feature selection based on information theory and feature ranking. *Knowl. Based Syst.* **2018**, *140*, 103–119. [[CrossRef](#)]
85. Bidar, M.; Sadaoui, S.; Mouhoub, M.; Bidar, M. Enhanced firefly algorithm using fuzzy parameter tuner. *Comput. Inf. Sci.* **2018**, *11*, 26–51. [[CrossRef](#)]
86. Mai, S.H.; Seghier, M.E.A.B.; Nguyen, P.L.; Jafari-Asl, J.; Thai, D.-K. A hybrid model for predicting the axial compression capacity of square concrete-filled steel tubular columns. *Eng. Comput.* **2020**, 1–18. [[CrossRef](#)]
87. Wang, Y.; Geng, Y.; Ranzi, G.; Zhang, S. Time-dependent behaviour of expansive concrete-filled steel tubular columns. *J. Constr. Steel Res.* **2011**, *67*, 471–483. [[CrossRef](#)]
88. Geng, Y.; Wang, Y.; Chen, J. Time-dependent behaviour of steel tubular columns filled with recycled coarse aggregate concrete. *J. Constr. Steel Res.* **2016**, *122*, 455–468. [[CrossRef](#)]
89. Dong, J.F.; Wang, Q.Y.; Guan, Z.W. Structural behaviour of recycled aggregate concrete filled steel tube columns strengthened by CFRP. *Eng. Struct.* **2013**, *48*, 532–542. [[CrossRef](#)]
90. Wang, Y.; Chen, J.; Geng, Y. Testing and analysis of axially loaded normal-strength recycled aggregate concrete filled steel tubular stub columns. *Eng. Struct.* **2015**, *86*, 192–212. [[CrossRef](#)]
91. Chen, J.; Wang, Y.; Roeder, C.W.; Ma, J. Behavior of normal-strength recycled aggregate concrete filled steel tubes under combined loading. *Eng. Struct.* **2017**, *130*, 23–40. [[CrossRef](#)]
92. Yang, Y.-F.; Ma, G.-L. Experimental behaviour of recycled aggregate concrete filled stainless steel tube stub columns and beams. *Thin-Walled Struct.* **2013**, *66*, 62–75. [[CrossRef](#)]
93. Wang, Y.; Geng, Y.; Chang, Y.; Zhou, C. Time-dependent behaviour of recycled concrete filled steel tubes using RCA from different parent waste material. *Constr. Build. Mater.* **2018**, *193*, 230–243. [[CrossRef](#)]
94. Wei, J.; Luo, X.; Lai, Z.; Varma, A.H. Experimental behavior and design of high-strength circular concrete-filled steel tube short columns. *J. Struct. Eng.* **2020**, *146*, 4019184. [[CrossRef](#)]
95. Le Hoang, A.; Fehling, E. Numerical study of circular steel tube confined concrete (STCC) stub columns. *J. Constr. Steel Res.* **2017**, *136*, 238–255. [[CrossRef](#)]
96. He, L.; Zhao, Y.; Lin, S. Experimental study on axially compressed circular CFST columns with improved confinement effect. *J. Constr. Steel Res.* **2018**, *140*, 74–81. [[CrossRef](#)]
97. Koopialipoor, M.; Jahed Armaghani, D.; Haghghi, M.; Ghaleini, E.N. A neuro-genetic predictive model to approximate overbreak induced by drilling and blasting operation in tunnels. *Bull. Eng. Geol. Environ.* **2017**, *78*, 981–990. [[CrossRef](#)]
98. Koopialipoor, M.; Ghaleini, E.N.; Tootoonchi, H.; Jahed Armaghani, D.; Haghghi, M.; Hedayat, A. Developing a new intelligent technique to predict overbreak in tunnels using an artificial bee colony-based ANN. *Environ. Earth Sci.* **2019**, *78*, 165. [[CrossRef](#)]
99. Yu, C.; Koopialipoor, M.; Murlidhar, B.R.; Mohammed, A.S.; Armaghani, D.J.; Mohamad, E.T.; Wang, Z. Optimal ELM–Harris Hawks optimization and ELM–Grasshopper optimization models to forecast peak particle velocity resulting from mine blasting. *Nat. Resour. Res.* **2021**, *30*, 2647–2662. [[CrossRef](#)]
100. Koopialipoor, M.; Nikouei, S.S.; Marto, A.; Fahimifar, A.; Armaghani, D.J.; Mohamad, E.T. Predicting tunnel boring machine performance through a new model based on the group method of data handling. *Bull. Eng. Geol. Environ.* **2018**, *78*, 3799–3813. [[CrossRef](#)]
101. Armaghani, D.J.; Koopialipoor, M.; Bahri, M.; Hasanipanah, M.; Tahir, M.M. A SVR-GWO technique to minimize flyrock distance resulting from blasting. *Bull. Eng. Geol. Environ.* **2020**, *79*, 4369–4385. [[CrossRef](#)]
102. Armaghani, D.J.; Yagiz, S.; Mohamad, E.T.; Zhou, J. Prediction of TBM performance in fresh through weathered granite using empirical and statistical approaches. *Tunn. Undergr. Space Technol.* **2021**, *118*, 104183. [[CrossRef](#)]